Effects of geometry of soil specimens on the formation of desiccation cracks

Yew Heng Sherman Seah[1], and *Eng Choon* Leong[1#]

[1]*Nanyang Technological University, School of Civil and Environmental Engineering, 50 Nanyang Avenue, 639798, Singapore*
[#]*Corresponding author: cecleong@ntu.edu.sg*

ABSTRACT

Desiccation cracks in soils are important in engineering structures that need hydraulic integrity such as earth dams, and containment facilities. At the element test level, such cracks are a hindrance when the volume change of the soil specimen needs to be measured during the test. One such test is the volumetric shrinkage test where the volume of the soil specimen needs to be continuously determined together with its mass change as the soil specimen dries. The soil specimen may deform non-uniformly. Previously hazardous and cumbersome methods using mercury or wax are needed to determine the volume of soil specimens that deform non-uniformly, but the advent of 3D scanning and photogrammetry enables the volume of non-uniform soil specimens to be measured quite accurately. However, such techniques cannot accurately determine the volume of the deformed soil specimen once cracks start appearing in the soil specimen. Volumetric shrinkage tests are commonly conducted for cylindrical soil specimens. This paper investigates the geometry (shapes and dimensions) of soil specimens other than cylindrical on the formation of desiccation cracks. Bentonite is used as the test soil as it experiences large volume change on drying. The test results provide guidance for the geometry of a soil specimen to be used in the volumetric shrinkage test.

Keywords: desiccation cracks; soil specimen; geometry; expansive soils

1. Introduction

In nature, soils in arid, semi-arid and semi-humid regions are more prone to desiccation cracks. Desiccation of soil occurs, and shrinkage cracks formed as water is evaporated from the surface of clayey soils. The volume of the soil shrinks as it dries, creating an even distribution of tensile stresses throughout the bedding plane. Desiccation cracks that form on the soil's surface relieve this tensile stress (Tanner 2003). When desiccation cracks are observed, it is noticed that the crack lines form polygonal soil clods that can be categorised into different morphologies.

In the laboratory, the standard shape of soil specimens used in soil tests is a circular shape. This is understandable because soils are usually collected in sampling tubes. Circular-shaped specimens are also easy to prepare using a ring cookie cutter. This includes the one-dimensional consolidation test with an oedometer (ASTM D2435-11 2020), pressure plate extractor test (ASTM D6836-16 2016) and others (ASTM D2166/D2166M-16 2016; ASTM D2850-15 2016; ASTM D4767-11 2020). When such soil specimens are subjected to drying, desiccation cracks are observed on the circular-shaped soil specimens especially when the soil contains expansive clay minerals such as smectite similar to those seen in nature. Volumetric shrinkage results in desiccation cracks on the surfaces which translate to inaccuracies when measuring the specimens' volume. Volumetric shrinkage of soils is usually measured by destructive means of testing such as paraffin wax (ASTM D4943-08 2021) or mercury intrusion test methods (ASTM D427-04 2004). However, these destructive testing methods mean that many identical soil specimens are needed to obtain a shrinkage curve showing the void ratio of the soil specimen at water contents from saturated to dry. A proposed solution is to rely on new technologies for non-destructive means of measuring the volume of the soil specimen. With advancements in camera optics and software programs, it has been suggested that digital imaging technology can quantify the volumetric shrinkage of the soil specimen (Puppala et al. 2004). Non-destructive means of testing would allow a single soil specimen to be used to determine the shrinkage curve.

Table 1 summarises the various methods that were proposed to determine soil volume in the laboratory. Non-contact means such as image analysis, laser, and 3D optical scans are the least intrusive means of measuring the volume by not adding additives to the surface of the material which might alter the rate of drying or osmotic transfer of water and air. However, the voids from the cracks within the soil specimen would be difficult to quantify.

Despite the various means of quantifying the volumetric shrinkage of cylindrical soil specimens (destructive and non-destructive methods), there has been a lack of study as to how other geometrical shapes of soil specimens could potentially reduce desiccation cracks in soil specimen. Reducing or eliminating the desiccation cracks from forming in the first place will eliminate the use of tedious methods as listed in Table 1. In turn, these specimens will not require complex methods to quantify the volume of the cracks present which translates to higher volume measurement accuracy

and the volume measurement can be achieved with ease and without requiring other specialised laboratory equipment or methods.

Surface desiccation cracks of soils in nature were observed to form cells of three to six sides with four to six sides being the most common (Tanner 2003). Taking the cue from nature, volumetric shrinkage experiments were conducted on soil specimens of different geometrical shapes. In this paper, various geometries such as cuboid (square cross-section), pentagon prism (pentagon cross-section), hexagon prism (hexagon cross-section), and disc (circular cross-section) were studied. The aim is to determine which geometries will result in the least cracks formation and serve as the preferred geometry when conducting volumetric shrinkage test for soils, especially expansive soils.

Adopting a multi-prong approach to determine the volume might be beneficial not just as a means of checking but also to improve the accuracy of volume measurement of a soil specimen on drying. In this paper, image analysis using ImageJ (Schneider et al. 2012) and direct measurements were adopted. Image analysis with ImageJ was used for measuring the plan area and direct measurement using Vernier callipers for the thickness of the soil specimen.

2. Motivation

There is a lack of investigation into the effect of geometrical shapes on desiccation cracks in soil specimens. Goodman and Vahedifard (2022) investigated desiccation cracks on cuboid and disc compacted soil specimens. The thicknesses of the soil specimens that were investigated in the study are 5 cm, 10 cm, and 15 cm with cross-sectional area between 314.2 cm^2 to 324.0 cm^2. In the study conducted, evaporation for the side surface was prevented by insulation and only the top surface was exposed to drying to simulate field drying conditions. The side areas were not monitored continuously but were only evaluated at the end of the 48-hour testing period. Crack depth was evaluated with image processing software developed by Tang et al. (2008). The image processing software used was Crack Image Analysis System (CIAS) which was written as a MATLAB script.

This paper extends Goodman and Vahedifard's (2022) study to include more geometrical shapes for soil specimens and the soil specimens were prepared from a slurry-consolidated soil sample. The side areas of the soil specimens were also exposed for continuous drying so that the shrinkage on the plan surface area and the thickness of the soil specimen can be monitored.

3. Materials and methods

The soil used in this study was commercial bentonite procured from International Scientific (Pte) Ltd, Singapore. Bentonite was chosen as it has high swelling and shrinkage properties, making it an ideal soil to investigate desiccation crack development of a soil specimen on drying.

Table 1. Quantification of soil specimens' volume in the laboratory

Method	Description	References
Mercury displacement method	-	ASTM D427-04 1998 (Withdrawn)
Paraffin wax method	-	ASTM D4943 2008; ASTM D7263 2009
Non-wetting fluids	By using kerdane oil	Fleureau et al, 1993
Water-repellent encasement method	By coating specimen with Methyl ethyl ketone (MEK) Saran	Nelson and Miller 1992; Crescimanno and Provenzano 1999
	By coating specimen with waterproof polyvinyl acetate-based adhesives (Elmer's craft glue)	Krosley at al. 2003
	By coating specimen with automotive varnish	De Almeida et al. 2009
	Hand-spray plaster as an encasement then immersed in silicon oil	Liu and Buzzi 2014
Image Analysis	Determination of areas and perimeter of the images in pixels	Puppala et al. 2004
	Particle image velocimetry (PIV) technique	Lu and Kaya 2013
	Specimen was coated with MEK and imaged using the Clodometer	Stewart et al. 2014
	3D photogrammetry with glitters	Wijaya et al. 2015
	Particle image velocimetry (PIV) technique	Dong and Lu 2017
Laser	Laser scanning with software	Rossi et al. 2008
3D optical scan	Photogrammetric methods	Sander and Gerke 2007
Balloon method	Specimen is placed in a balloon	Tariq and Durnford 1993
Direct measurement	Callipers	Péron et al. 2009

Table 2. Basic properties of bentonite from manufacturer

Parameter	Results
Moisture	13.4 % by wt.
pH	10.11
Free Swelling	31 ml
Liquid Limit	534%
MBA Value	426.36
Filtrate Loss	15.6 ml
Marsh Cone Viscosity	43 s
Specific Gravity*	2.77

*Determined in this study

3.1. Bentonite

The bentonite used is fine-grained with 100% passing through a 0.075 mm (No. 200) sieve. The physical characteristics of bentonite and its corresponding index properties are listed in Table 2. The specific gravity test was done in accordance with ASTM D854-14.

3.2. Methods

In this paper, A1 will be used to denote the area of the flat surface in the plan-view and A2 will be used to denote the side area perpendicular to A1. Two test series were investigated in this study. The first test series were soil specimens where the ratio A1:A2 is 1:1, and the second test series were soil specimens where the ratio A1:A2 is 1:2.

The geometries that were studied in this paper includes disc, cuboid, pentagon prism and hexagon prism. The corresponding A1 would be in the shape of a circle, square, hexagon and pentagon, respectively, as shown in Table 3. To compare the specimens, A1 for all the geometries was targeted at 25cm^2 with a maximum 1% variation and the A2 area has a maximum variation of 13.6% across the various geometries. The areas, A1 and A2, for the various specimen shapes are shown in Table 3.

A soil slurry was first prepared by mixing distilled water and bentonite uniformly in a mixer. The mass of water to mass of dry bentonite ratio was about 8:1. The slurry was allowed to rest for at least 24 hours to ensure that the bentonite has fully absorbed the water. The slurry was stirred and then carefully placed into a 30 cm internal diameter consolidation tank where a piece of filter paper was placed at the bottom of the consolidation tank. During the transfer of the slurry into the consolidation tank, it was ensured that air bubbles were not trapped within the soil slurry. A piece of filter paper was also placed on top of the slurry before closing the consolidation tank.

The consolidation pressure applied to consolidate the soil slurry was 120 kPa. The consolidation process took between five to seven days for the soil to be fully consolidated depending on the thickness of the sample. The sample was then extruded out of the consolidation tank and the geometric shapes were cut with a sharp long blade cutter using a 3D printed geometric shapes template. Lubricating oil was used to thinly coat the surface of the cutter to reduce friction during the cutting process. The soil specimens were then transferred onto acrylic tiles that measure about 105 mm x 70 mm x 5 mm thickness. The surface of the acrylic tile is smooth with negligible friction that might impede the shrinkage of the bottom part of the soil specimen on drying.

To standardize the drying process, the soil specimens were subjected to multiple cycles of drying and cooling in a 50℃ oven. They were placed in the oven for 15 minutes and left to cool for 15 mins. The soil specimens were then weighed and photographed from the top and side of the specimen. Vernier callipers was used to obtain the thickness of the soil specimen at four points without handling the soil specimen. The oven was also pre-set with medium fan speed to allow for even air circulation. The process was stopped when there was no significant decrease in weight. Finally, the specimen was dried in the oven at 105℃ for 24 hours to obtain its final moisture content.

The images of the plan view of the specimens were processed using ImageJ to obtain the plan area, A1. The images were first adjusted for the colour threshold to turn it into binary images of black and white. The area was then calculated by ImageJ based on pixels. The thickness of the soil specimens was determined using Vernier callipers. Four measurements along the sides were taken, with two largest thicknesses and two smallest thicknesses, and the average thickness was calculated. The volume of the soil specimen was determined as average thickness multiplied by plan area, A1.

Table 3. Test series 1 and 2 for the ratio A1:A2 of 1:1 and 1:2, respectively

Test Series	Shape	A1 (cm^2)	A2 (cm^2)
1	Disc	24.6	32.0
	Hexagon Prism	25.0	32.5
	Pentagon Prism	24.8	32.3
	Cuboid	25.0	32.5
2	Disc	24.6	61.6
	Hexagon Prism	25.0	62.4
	Pentagon Prism	24.8	62.1
	Cuboid	25.0	62.5

4. Results and discussion

4.1. Volumetric Shrinkage

From the volume of the soil specimen, its void ratio was calculated for the prevailing water content. The data were then plotted on a void ratio versus water content graph. This forms the shrinkage curve for each geometry. Figs. 1 and 2 show the combined plot of the shrinkage curves for the four geometries of test series 1 and 2, respectively.

For test series 1, the disc, hexagon prism and cuboid specimens have relatively the same minimum void ratio, e_{min}, whereas the pentagon prism specimen was observed to have the smallest e_{min} value. Pentagon prism specimen experiences desiccation cracks only towards the end of drying. Most of the data for the pentagon prism specimen lies on the 100% degree of saturation line. Deviation from the 100% degree of saturation lines occurs when desiccation cracks form on the side faces, A2. This is also reflected in the shrinkage curve in Fig. 2.

For test series 2, the disc specimen has the greatest deformation and desiccation cracks, and hence the largest minimum void ratio, e_{min}. The pentagon prism specimen has the smallest e_{min}. The pentagon prism specimen experiences desiccation cracks only towards the end of drying. This is also reflected in the water content versus void ratio graph in Fig. 2. Likewise, for test series 2, most of the shrinkage curve data for the pentagon prism specimen lies on the 100% degree of saturation line. Deviation from the 100% degree of saturation lines occurs when desiccation cracks formed. Both the hexagon prism specimen and the cuboid specimen's e_{min} falls between the disc and the pentagon prism specimens.

Hence, it might suggest that the pentagon prism specimen has the most suitable geometry to determine the shrinkage curve for bentonite. In addition, although the specimens with A1:A2 ratio of 1:1 have consistently lower e_{min} value, the difficulty in handling the soil specimens with A1:A2 ratio of 1:1 was greater as the desiccation cracks propagate inwards and result in breakage of cracks resulting in loose pieces of dried soil pieces. Greater care must be taken for using specimens with A1:A2 ratio of 1:1. Hence, it is recommended that specimens with ratio A1:A2 of 1:2 should be used for the ease of handling.

Goodman and Vahedifard (2022) made two observations in their study:

1. By increasing the soil specimen's thickness, surface crack ratio, crack length and crack width increase.
2. After surface crack ratio peaked, disc specimens have consistently larger surface crack ratio as compared to cuboid specimens of different thicknesses.

In this study, it was ascertained that increasing soil specimen thickness, does increase the crack length and crack width. However, the surface area that is cracked was not investigated.

4.2. Crack development

Four moisture contents for each geometry were selected for illustration of development of cracks during the drying process. These data are indicated by the filled symbols in Figs. 1 and 2. The data for each geometry at similar moisture content are grouped into Groups 1 to 4. Group 1 images were taken before oven drying. Group 4 images were taken after drying at 105ºC in the oven for 24 hours. Groups 2 and 3 were taken during the process of drying at 50ºC in the oven.

Plan and side view images of the soil specimens at four moisture contents (Groups 1 to 4) are summarised in Figs. 4 to 7 for test series 1 and Figs. 8 to 11 for test series 2. Based on Figs. 4 to 11, it was observed that fewer and less severe cracks occur on the surface area A1 compared to the side area A2. This observation indicates that the horizontal cracks on side area A2 have lower energy than the vertical cracks on surface area A1.

From Figs. 6 and 10 before final oven drying at 105ºC, the disc specimen showed the largest and greatest desiccation cracks on side area A2 which propagates as drying progresses. The hexagon prism specimen and cuboid specimen also exhibited some slight cracking, whereas the pentagon prism specimen has the least cracks on plan area A1 and side area A2.

After 105ºC drying in the oven for at least 24 hours, the horizontal cracks appear to separate the soil specimens into two to three horizontal layers as can be seen in Figs. 7 and 11. Distortion of plan area A1 shape was also noticeable for the disc, hexagon prism and cuboid whereas for the pentagon prism specimen, the plan area A1 remains relatively flat with minimal shape distortion.

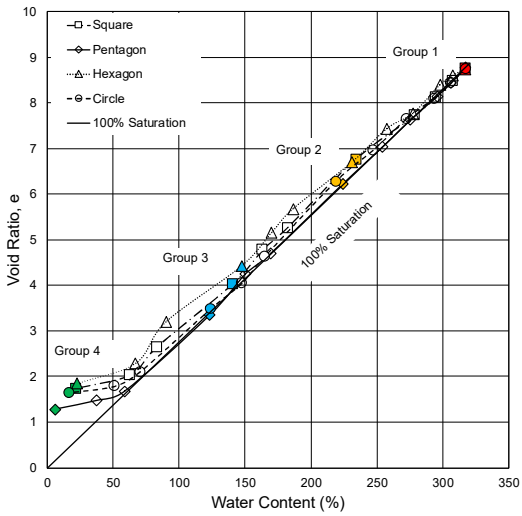

Figure 1. Shrinkage curves for test series 1.

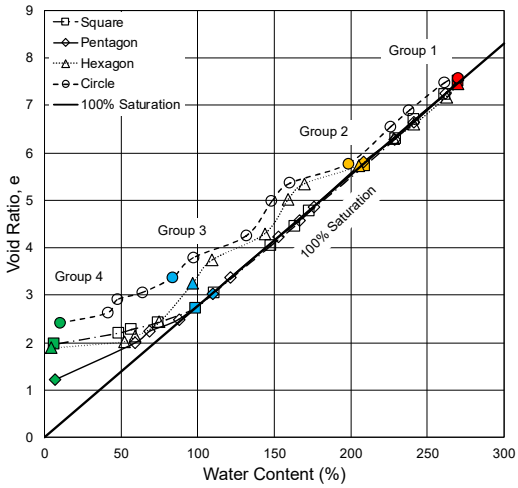

Figure 2. Shrinkage curves for test series 2.

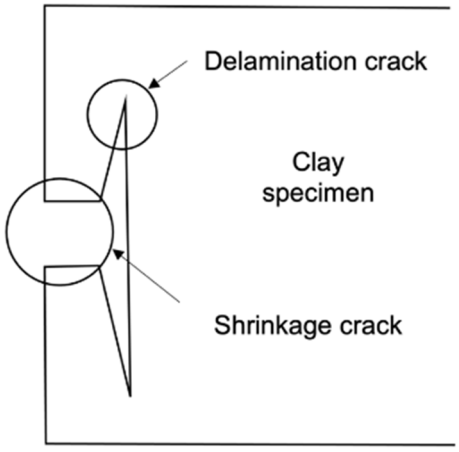

Figure 3. Crack formation of a drying clay specimen (Modified from Bohn et al. 2005).

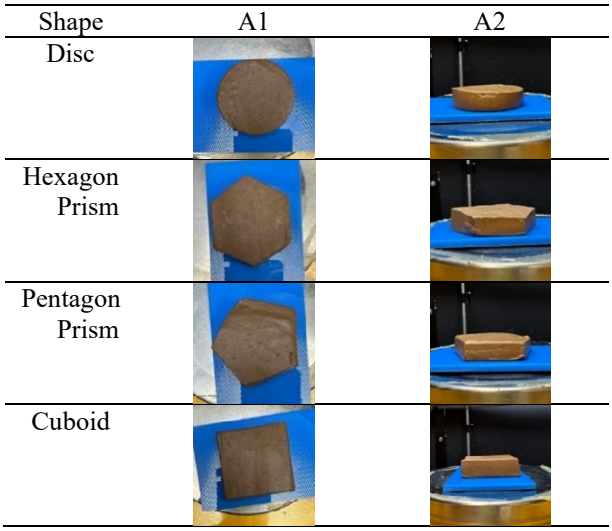

Figure 4. Test series 1-group 1 specimens with the corresponding A1 and A2 images.

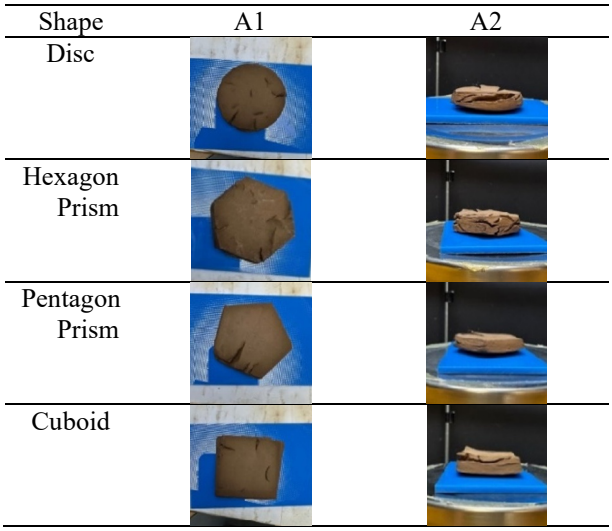

Figure 5. Test series 1-group 2 specimens with the corresponding A1 and A2 images.

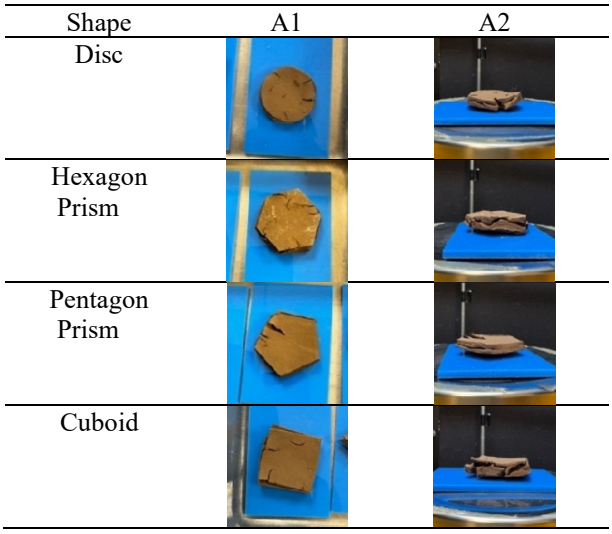

Figure 6. Test series 1-group 3 specimens with the corresponding A1 and A2 images.

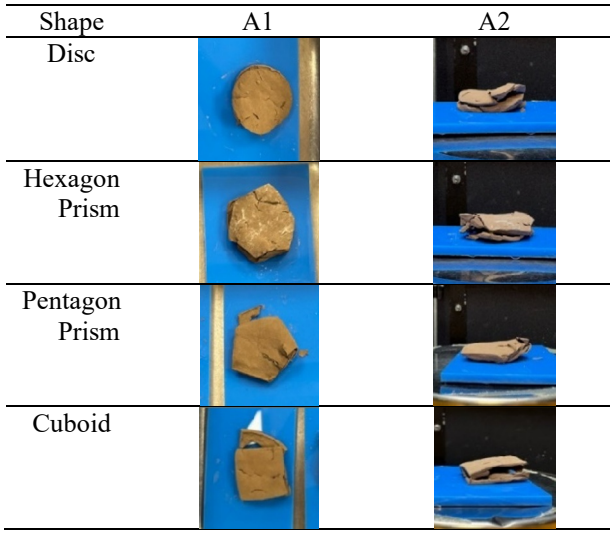

Figure 7. Test series 1-group 4 specimens with the corresponding A1 and A2 images.

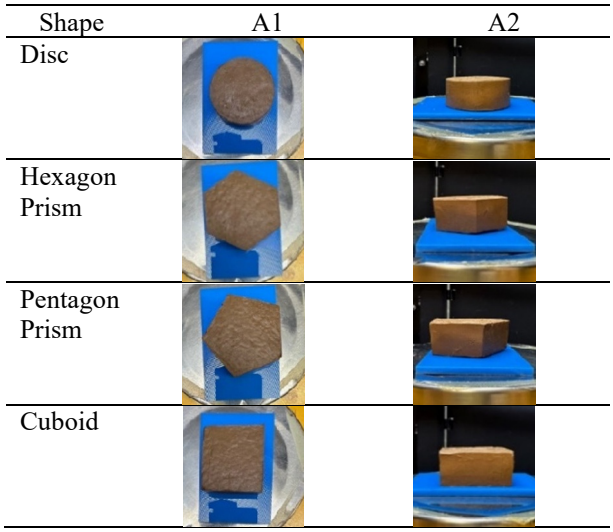

Figure 8. Test series 2-group 1 specimens with the corresponding A1 and A2 images.

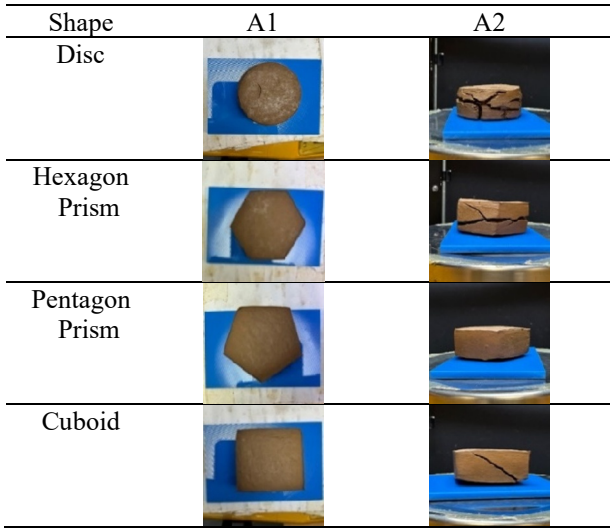

Figure 9. Test series 2-group 2 specimens with the corresponding A1 and A2 images.

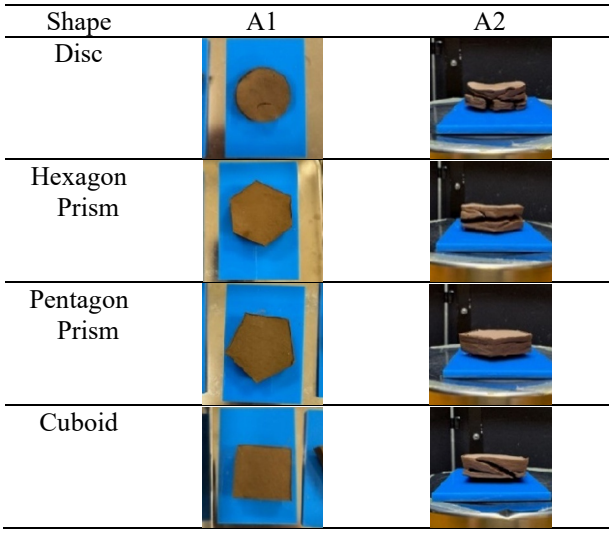

Figure 10. Test series 2-group 3 specimens with the corresponding A1 and A2 images.

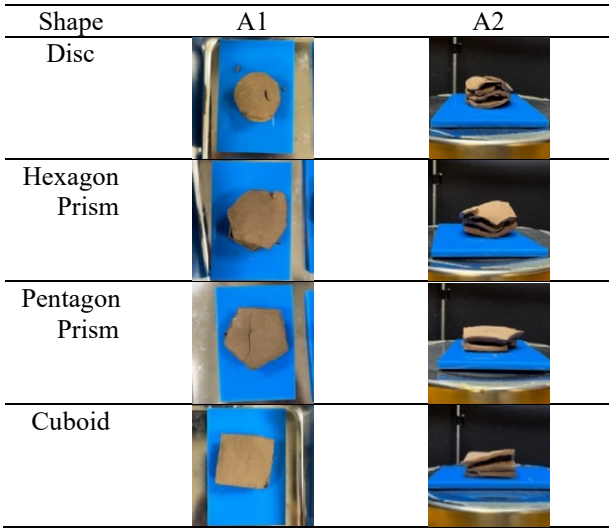

Figure 11. Test series 2-group 4 specimens with the corresponding A1 and A2 images.

The development of horizontal cracks observed on the side area A2 is described by Bohn et al. (2005) as a delaminated fracture that has opened and is known as a mud peel process. Tensile stresses are developed at the clay's surface during drying, which can result in shrinkage cracks perpendicular to the clay's surface. Once a shrinkage crack has formed, delamination cracks that migrate sideways from the shrinkage crack may appear. However, it need not be parallel to the drying surface as shown in Fig. 3.

For both test series 1 and 2, the soil specimens exhibited delaminated fracture resulting in the soil specimen after oven drying showing one to three horizontal layers as summarised in Table 4.

The pentagon prism specimen was observed to show the least number of horizontal layers compared to other geometries for each test series even though the initial thicknesses of the specimens were identical. According to Bohn et al. (2005), the clay remains saturated with water during the early stage of drying due to soil particle consolidation caused by lowering water pressure in the clay's pores. Tensile stresses arise at this stage, which can lead to primary, craquelure-type cracking.

The maximum tensile stresses capable of causing an initial fracture exists before desaturation, and crack development begins when the material is completely saturated. Bohn et al. (2005) findings are consistent with Tang et al. (2011) findings that during the normal shrinkage phase of a Soil-Shrinkage Characteristic Curve (SSCC), 80% of the cracks will be formed in this phase. Based on the volumetric shrinkage curves in Figs. 1 and 2, the shrinkage curve of the specimen starts to deviate from the 100% saturation line when desiccation cracks were formed. This was more pronounced in test series 2 which has a greater specimen thickness and was more prominent in geometries such as disc and hexagon prism specimens which showed more desiccation cracks.

4.3. Shrinkage curve equation

Fredlund et al. (2002) proposed that the shrinkage curve can be represented by Equation 1.

$$e = a_{sh}\left[\frac{w^{c_{sh}}}{b_{sh}{}^{c_{sh}}} + 1\right]^{\frac{1}{c_{sh}}} \quad (1)$$

where a_{sh} denotes the minimum void ratio, e_{min}; b_{sh} denotes the slope of the line of tangency; c_{sh} denotes the curvature of the shrinkage curve; $\frac{a_{sh}}{b_{sh}} = \frac{G_s}{S}$ = constant for a specific soil; G_s denotes the specific gravity of the soil and S denotes the degree of saturation.

Test series 1 and 2 shrinkage curve data for the four geometries were curve-fitted with Equation 1 as shown in Figs. 12 to 15. Microsoft Excel Solver was used to obtain parameters a_{sh}, b_{sh} and c_{sh} as summarised in Table 5. Based on Table 5, the pentagon prism specimens for both test series 1 and 2 have similar values for a_{sh}, b_{sh} and c_{sh} due to e_{min} being similar for both thicknesses. However, the geometry with the greatest difference in the parameters for test series 1 and 2 is the disc. This is due to the significant difference in e_{min} value disc specimens of test series 1 and 2. Fredlund et al. (2002) mentioned that curve-fitting provides a good basis for estimating volumetric shrinkage of expansive soil where quantification of volume might be difficult. The experimental data agree with the findings of Fredlund et al. (2002).

Table 4. Number of mud peel layers in test series 1 and 2 based on group 4

Test Series	Shape	Number of layers
1	Disc	2
	Hexagon Prism	2
	Pentagon Prism	1
	Cuboid	2
2	Disc	3
	Hexagon Prism	3
	Pentagon Prism	2
	Cuboid	3

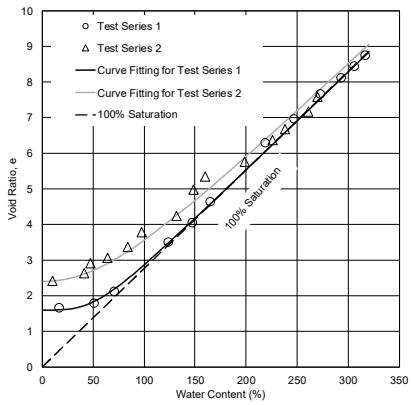

Figure 12. Test series 1 and 2 for disc specimen fitted with Fredlund et al. (2002) equation.

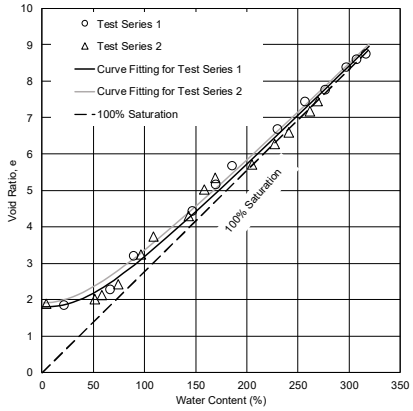

Figure 13. Test series 1 and 2 for hexagon prism specimen fitted with Fredlund et al. (2002) equation.

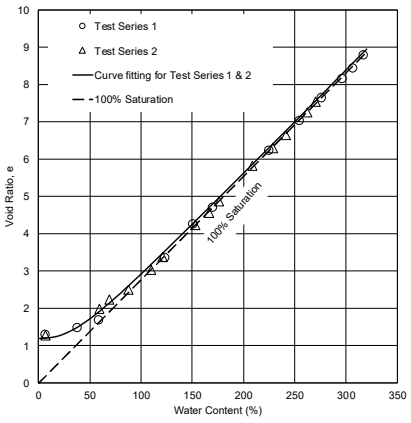

Figure 14. Test series 1 and 2 for pentagon prism specimen fitted with Fredlund et al. (2002) equation.

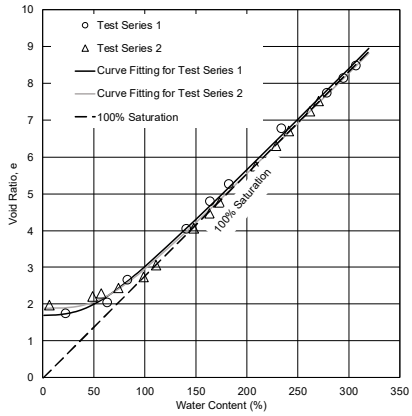

Figure 15. Test series 1 and 2 for cuboid specimen fitted with Fredlund et al. (2002) equation.

Table 5. Parameters a_{sh}, b_{sh}, c_{sh} for the four geometries and the corresponding test series

Shape	Test Series	a_{sh} (e_{min})	b_{sh}	c_{sh}
Disc	1	1.6	58	3.5
	2	2.4	87	2.2
Hexagon Prism	1	1.8	65	2.3
	2	1.9	69	2
Pentagon Prism	1	1.2	43	2.5
	2	1.2	43	2.5
Cuboid	1	1.7	61	2.8
	2	1.9	69	3.4

5. Conclusion and future works

5.1. Conclusion

In conclusion, several specimen geometries (disc, cuboid, pentagon prism and hexagon prism) for the determination of the shrinkage curve of bentonite were investigated in this study. The pentagon prism specimens exhibited the fewest desiccation cracks as compared to the other geometries. The pentagon prism specimens also exhibited fewer delaminated-fractured horizontal layers as compared to other geometries. The thickness of the soil specimens also affected the development of desiccation cracks. It was found that specimen ratio A1: A2 of 1:2 is more advantageous than specimen ratio A1:A2 of 1:1 as the soil specimens were easier to handle since the desiccation cracks would be less prone to breakage. Hence, it is recommended that the pentagon prism specimen may be a better specimen shape to use when conducting a volumetric shrinkage test compared to the usual disc specimen. The reason for the higher resistance of the pentagon prism soil specimen to desiccation cracking is currently being further investigated. However, the observation for the pentagon prism bentonite specimen should also apply to other soil types as bentonite undergoes large volume change during drying and represent the extreme condition for clayey soils.

5.2. Future works

Desiccation cracks are complex problems that can be attributed to multiple factors such as relative humidity, soil composition, thickness, temperature, and suction. The effect of desiccation cracks on soil specimens is still not well understood. This study represents one of the few studies which investigated the effect of geometry and thickness of the soil specimen on desiccation cracks.

Acknowledgements

The authors would like to acknowledge funding support for this research project is obtained from Nanyang Technological University, Singapore, for Undergraduate Research on Campus (URECA) Programme.

References

ASTM "D2435-11: Standard Test Methods for One-Dimensional Consolidation Properties of Soils Using

Incremental Loading," ASTM International, West Conshohocken, PA, USA, 2012, https://doi.org/10.1520/D2435_D2435M-11R20

ASTM "D6836-16: Standard Test Methods for Determination of the Soil Water Characteristic Curve for Desorption Using Hanging Column, Pressure Extractor, Chilled Mirror Hygrometer, or Centrifuge," ASTM International, West Conshohocken, PA, USA, 2016, https://doi.org/10.1520/D6836-16

ASTM "D427-04: Standard Test Method for Shrinkage Factors of Soils by the Mercury Method," ASTM International, West Conshohocken, PA, USA, 2004, https://doi.org/10.1520/D427-04

ASTM "D4943-08: Standard Test Method for Shrinkage Factors of Soils by the Wax Method," ASTM International, West Conshohocken, PA, USA, 2008, https://doi.org/10.1520/D4943-08

ASTM "D2216-10: Standard Test Methods for Laboratory Determination of Water (Moisture) Content of Soil and Rock by Mass," ASTM International, West Conshohocken, PA, USA, 2010, https://doi.org/10.1520/D2216-10

ASTM "D854-14: Standard Test Method for Specific Gravity of Soils," ASTM International, West Conshohocken, PA, USA, 2014, https://doi.org/10.1520/D0854-14

BS "1377: Methods of Test for Soils for Civil Engineering Purposes, Part 2." British Standards Institution, London, 1990.

Bohn, S., Pauchard, L., Couder, Y. "Hierarchical crack pattern as formed by successive domain divisions. I. Temporal and geometrical hierarchy," Phys. Rev. E, Vol. (71), 046214. 2005. https://doi.org/10.1103/PhysRevE.71.046214

Goodman, C.C., Vahedifard, F. "Effects of sample thickness and shape on cracking patterns and crack depth in a compacted clay." In: Geo-Congress 2022, USA. https://doi.org/10.1061/9780784484050.018

Crescimanno, G., Provenzano, G. "Soil shrinkage characteristic curve in clay soils: measurement and prediction." Soil Sci Soc Am J, Vol. (63), pp. 25-32, 1999. https://doi.org/10.2136/sssaj1999.03615995006300010005x

de Almeida, B.G., da Silva, A.P., Raine, S.R., Figueiredo, G.C. "Evaluation of automotive varnish as a coating for density measurements of soil clods." Soil Sci Soc Am J, Vol. (73), pp. 449–452, 2009. https://doi.org/10.2136/sssaj2008.0191

Dong, Y., Lu, N. "Measurement of suction-stress characteristic curve under drying and wetting conditions." Geotech Test J, Volume (40), pp. 107–121. 2017. http://dx.doi.org/10.1520/GTJ20160058

Fleureau, J.M., Kheirbek-Saoud, S., Soemitro, R., Taibi, S. "Behaviour of clayey soils on drying- wetting paths." Can Geotech J, Volume (30), pp. 287–296, 1993. https://doi.org/10.1139/t93-024

Fredlund, M.D., Wilson, G.W., Fredlund, D.G. "Representation and estimation of the shrinkage curve." In: Proc 3rd Int Conf on Unsaturated Soils, pp. 145–149, 2002.

Krosley, L., Lu, N., Likos, W.J. "Alternative encasement materials for clod test." Geotech Test J, Volume (26), pp. 1–3, 2003. https://doi.org/10.1520/GTJ11259J

Nelson, J.D., Miller, D.J., "Expansive Soils." Willy, New York, 1992. https://doi.org/10.1520/GTJ20130091

Liu, X., Buzzi, O. "Use of hand-spray plaster as a coating for soil bulk volume measurement." Geotech Test J, Volume (37), pp. 1–7. 2014. https://doi.org/10.1520/GTJ20130091

Lu, N., Kaya, M. "A drying cake method for measuring suction-stress characteristic curve, soil–water-retention curve, and hydraulic conductivity function." Geotech Test J, Volume (36), pp. 1–19, 2013. https://doi.org/10.1520/GTJ20120097

Puppala, A.J., Balakrishna, K., Hoyos, Laureano R. "Volumetric shrinkage strain measurements in expansive soils using digital imaging technology." Geotech Test J Volume (27), pp. 1–10. 2004. https://doi.org/10.1520/GTJ12069

Rossi, A.M., Hirmas, D.R., Graham, R.C., Sternberg, P.D. "Bulk density determination by automated three-dimensional laser scanning." Soil Sci Soc Am J, Volume (72), pp. 1591-1593, 2008. https://doi.org/10.2136/sssaj2008.0072N

Sander, T., Gerke, H. H. "Noncontact shrinkage curve determination for soil clods and aggregates by three-dimensional optical scanning." Soil Sci Soc Am J, Volume (71), pp. 1448-1454, 2007. https://doi.org/10.2136/sssaj2006.0372

Schneider, C.A., Rasband, W.S., Eliceiri, K.W. "NIH Image to ImageJ: 25 years of image analysis." Nature Methods, Volume (9), pp. 671–675, 2012. https://doi.org/10.1038/nmeth.2089

Stewart, R.D., Abou Najm, M.R., Rupp, D.E., Selker, J.S. "An image-based method for determining bulk density and the soil shrinkage curve." Soil Sci Soc Am J, Volume (76), pp. 1217–1221, 2012. https://doi.org/10.2136/sssaj2011.0276n

Style, R.W., Peppin, S.S.L. Cocks. A.C.F. "Mud peeling and horizontal crack formation in drying clays." J Geophys Res, Volume (116), F01025, 2011. https://doi.org/10.1029/2010JF001842

Tang, C.S., Shi, B., Liu, C., Suo, W.B., Gao, L. "Experimental characterization of shrinkage and desiccation cracking in thin clay layer," Appl Clay Sci, Volume (52), pp. 69–77, 2011. https://doi.org/10.1016/j.clay.2011.01.032

Tariq, A.U.R., Durnford, D.S. "Soil volumetric shrinkage measurements. A simple method." Soil Sci., Vol. (155), pp. 325–330, 1993. https://doi.org/10.1097/00010694-199305000-00003

Wijaya, M., Leong, E.C., Rahardjo, H. 2015. "Effect of shrinkage on air-entry value of soils." Soils Found, Volume (55), pp. 166–180. https://doi.org/10.1016/j.sandf.2014.12.013

Péron, H., Hueckel, T., Laloui, L., Hu, L. "Fundamentals of desiccation cracking of fine-grained soils: experimental characterisation and mechanisms identification." Can Geotech J, Volume (46), pp. 1177–1201, 2009. https://doi.org/10.1139/T09-054

Puppala, A.J., Katha, B., and Hoyos, L.R. "Volumetric shrinkage strain measurements in expansive soils using digital imaging technology." Geotech Test J, Volume (27), pp. 547–556, 2004. https://doi.org/10.1520/GTJ12069

Tanner, P.W.G. "Desiccation structures (mud cracks, etc.)". In: Encyclopedia of Sediments and Sedimentary Rocks. Encyclopedia of Earth Sciences Series. Springer, Dordrecht, 1978. https://doi.org/10.1007/978-1-4020-3609-5_65